

FIG. 3 The lower panel shows the electron density ( $N$ ) determined from upper hybrid emissions in the vicinity of Ganymede. The upper panel shows the electron number density as a function of radial distance ( $R$ ). Note the close similarity of the inbound and outbound profiles, which indicates that Ganymede is surrounded by an ionosphere-like plasma envelope extending several thousand kilometres above the surface.

the vicinity of Ganymede probably play an important role in the generation of these emissions by bringing the resonance energy down into a range where there are high electron intensities.

The electrostatic upper hybrid waves and electron cyclotron waves are closely related and constitute a general class known as electron cyclotron harmonic (ECH) waves. ECH waves are also driven by an anisotropy in the electron velocity distribution, similar to the whistler-mode. However, the electron energies involved<sup>18</sup>, 10–100 eV, are usually much lower, and the origin of the anisotropy is quite different. Whereas absorption by a planetary body usually causes the anisotropy required to drive whistler-mode emissions, other factors usually cause the anisotropy required to produce electron cyclotron waves. For example, when electrons are convected into a region of strong magnetic field, the perpendicular energy is increased relative to the parallel energy ( $W_{\perp} > W_{\parallel}$ ), thereby producing the necessary anisotropy. The electron plasma frequency to cyclotron frequency ratio,  $f_p/f_c$ , also plays a crucial role<sup>17</sup>. This ratio varies considerably during the fly-by, which may explain why the whistler-mode waves and the electron cyclotron waves occur in different regions. Electron precipitation into Ganymede's atmosphere due to pitch-angle scattering by whistler-mode or ECH waves could cause observable optical emissions, possibly accounting for the auroral emissions recently observed near Ganymede by the Hubble Space Telescope<sup>26</sup>. □

Received 30 September; accepted 5 November 1996.

1. Johnson, T. V., Yeates, C. M. & Young, R. *Space Sci. Rev.* **60**, 3–21 (1992).
2. Gurnett, D. A. et al. *Space Sci. Rev.* **60**, 341–355 (1992).
3. Stix, T. H. *The Theory of Plasma Waves* 12 (McGraw-Hill, New York, 1962).
4. Kennel, C. F. & Petschek, H. E. *J. Geophys. Res.* **71**, 1–28 (1966).
5. Helliwell, R. A. *Whistlers and Related Ionospheric Phenomena* 207 (Stanford Univ. Press, Stanford, 1965).

6. Kurth, W. S. & Gurnett, D. A. *J. Geophys. Res.* **96**, 18977–18991 (1991).
7. Burtis, W. J. & Helliwell, R. A. *J. Geophys. Res.* **74**, 3002–3010 (1969).
8. Kivelson, M. G. et al. *Nature* **384**, 537–541 (1996).
9. Scarf, F. L., Gurnett, D. A. & Kurth, W. S. *Nature* **292**, 747–750 (1981).
10. Gurnett, D. A. et al. *J. Geophys. Res.* **84**, 7043–7058 (1979).
11. Walsh, D., Haddock, T. F. & Schulte, H. F. *Space Res.* **4**, 935–959 (1964).
12. Mosier, S. R., Kaiser, M. L. & Brown, L. W. *J. Geophys. Res.* **78**, 1673–1677 (1973).
13. Warwick, J. W. et al. *Science* **204**, 995–998 (1979).
14. Gurnett, D. A. *J. Geophys. Res.* **86**, 8199–8212 (1981).
15. Noll, K. S., Johnson, R. E., Lane, A. L., Domingua, D. L. & Weaver, H. A. *Science* **273**, 341–343 (1996).
16. Kennel, C. F., Scarf, F. L., Fredericks, R. W., McGehee, J. H. & Coroniti, F. V. *J. Geophys. Res.* **75**, 6136–6152 (1970).
17. Ashour-Abdalla, M., Chanteur, G. & Pellat, R. *J. Geophys. Res.* **80**, 2775–2782 (1975).
18. Rönnmark, K., Borg, H., Christiansen, P. J., Gough, M. P. & Jones, D. *Space Sci. Rev.* **22**, 401–417 (1978).
19. Gurnett, D. A. *J. Geophys. Res.* **80**, 2751–2763 (1975).
20. Gurnett, D. A. & Frank, L. A. *J. Geophys. Res.* **81**, 3875–3885 (1976).
21. Kaiser, M. L. & Desch, M. D. *J. Geophys. Res.* **87**, 389–392 (1980).
22. Melrose, D. B. *J. Geophys. Res.* **86**, 30–36 (1981).
23. Van Allen, J. A. et al. *Science* **183**, 309–311 (1974).
24. Krimigis, S. M. et al. *Science* **204**, 998–1003 (1979).
25. Lanzerotti, L. J. et al. *Science* **257**, 1518–1524 (1992).
26. Cowen, R. *Science News* **150**, 181 (1996).

ACKNOWLEDGEMENTS. We thank the Galileo project team at the Jet Propulsion Laboratory for their efforts in obtaining these data, and M. Kivelson for providing the magnetometer data. We also thank L. Granroth and J. Groene for their assistance in the data processing at The University of Iowa. This work was supported by NASA through the Jet Propulsion Laboratory, and by the Centre National d'Etudes Spatiales (France).

CORRESPONDENCE should be addressed to D.A.G. (donald-gurnett@uiowa.edu).

## Discovery of Ganymede's magnetic field by the Galileo spacecraft

M. G. Kivelson\*†, K. K. Khurana\*, C. T. Russell\*†, R. J. Walker\*, J. Warnecke\*, F. V. Coroniti‡, C. Polanskey§, D. J. Southwood\*|| & G. Schubert\*‡

\* Institute of Geophysics and Planetary Physics, † Department of Earth and Space Sciences, ‡ Department of Physics, University of California, Los Angeles, California 90095-1567, USA

§ Jet Propulsion Laboratory, 4800 Oak Grove Drive, Pasadena, California 91109, USA

|| Department of Physics, Imperial College of Science, Technology, and Medicine, London SW7 2BZ, UK

THE Galileo spacecraft has now passed close to Jupiter's largest moon—Ganymede—on two occasions, the first at an altitude of 838 km, and the second at an altitude of just 264 km. Here we report the discovery during these encounters of an internal magnetic field associated with Ganymede (the only other solid bodies in the Solar System known to have magnetic fields are Mercury, Earth and probably Io<sup>1</sup>). The data are consistent with a Ganymede-centred magnetic dipole tilted by  $\sim 10^\circ$  relative to the spin axis, and an equatorial surface-field strength of  $\sim 750$  nT. The magnetic field is strong enough to carve out a magnetosphere with clearly defined boundaries within Jupiter's magnetosphere. Although the observations require an internal field, they do not indicate its source. But the existence of an internal magnetic field should in itself help constrain models of Ganymede's interior.

On Galileo's first inbound pass following orbital insertion, the magnetometer<sup>2</sup> measurements followed reasonably closely the predictions from a recent model of the magnetic field of Jupiter's magnetosphere<sup>3</sup> that we refer to as the KK96 model. (This model consists of the O6 model<sup>4</sup> of Jupiter's internal field plus the field of a warped and hinged current sheet parametrized to fit the magnetic field measured on the Pioneer 10 outbound pass near the dawn meridian.) The field increased in magnitude with approach to Jupiter and varied in orientation at Jupiter's rotation period. Data from 00:00 UT (universal time; h:min) to 12:00 UT on

27 June 1996 are plotted in Fig. 1; the Ganymede-associated perturbation is clearly apparent at 06:29 UT. The Ganymede encounter occurred well off the jovian magnetic equator (identifiable by the reversal of sign of  $B_r$  (the coordinate system is defined in Fig. 1 legend)) and thus in a region of relatively low plasma density. Closest approach was downstream of Ganymede relative to the flowing plasma of Jupiter's magnetosphere. Near to Ganymede, the field increased from 107 nT at 06:00 UT to 480 nT at 06:29:07 UT (h:min:s) near closest approach, and then decreased to background, returning to 118 nT at ~07:00 UT. A considerable rotation accompanied the change in field magnitude.

The data near closest approach for this first pass are shown in Fig. 2. The field near closest approach is approximately that of a magnetic dipole centred at Ganymede with surface strength 750 nT at the equator added to the KK96 model. The dipole north pole is tilted by  $10^\circ$  from the spin axis towards  $200^\circ$  Ganymede east longitude. (Longitude of  $180^\circ$  is radially outward from Jupiter.) Currents flowing in the magnetospheric plasma in Ganymede's environment perturb the magnetic signature<sup>5,6</sup>, so the actual magnetic moment of Ganymede may be slightly overestimated by the vacuum field estimate. In Fig. 3 we show projections of the trajectory and of the perturbation field vectors measured along it. (The perturbation field is the vector difference between the observed field and the KK96 model field.) The figure illustrates that the field perturbations converge towards Ganymede, as expected in the vicinity of an internal dipole.

For the second pass, Ganymede was again located well above the jovian current sheet, probably in a region of low plasma density. The full data from the magnetometer and other particle and field instruments will be reported elsewhere, but measurements at ~1-minute resolution were acquired in advance of the full data set by operating the magnetometer<sup>2</sup> in a mode that averages and stores up to 200 field vectors for delayed transmission to the ground. Figure 4 presents these initial data and the vacuum field model previously described, which again provides a reasonable approximation to the data. Because of the low altitude of closest approach on this pass, the internal field dominates the signature (the field magnitude reached 1,146 nT at 18:59:45 on 6 September 1996). The small discrepancies between the data and the modelled field arise from various neglected effects. The vacuum superposition model does not allow for the fact that the external field is frozen into the flowing plasma of the jovian magnetosphere which modifies the interaction. In particular, currents that flow through the jovian plasma and close through Ganymede or a possible ionosphere<sup>5,6</sup> produce perturbations that tilt the field in the direction of the corotation flow. These neglected perturbations affect principally  $B_\phi$  (see Fig. 2 legend) which is poorly fitted by the model. Possible contributions from higher-order multipoles of the internal field have not been considered.

We have traced field lines near Ganymede in a simplified representation of the magnetic geometry (Fig. 5). The background (jovian) field is assumed uniform and tilted radially away from Jupiter. It has been added to the field of a Ganymede dipole pointing to  $10^\circ$  radially inward relative to the southward direction (which is the same as tilting the

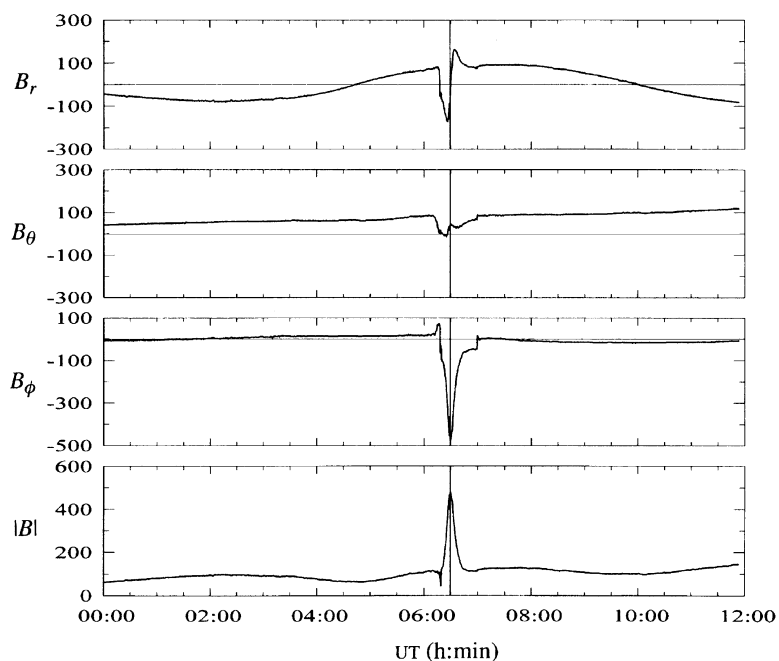


FIG. 1 Magnetometer data for the inbound pass to Jupiter on 27 June 1996 over a radial distance range from 17.44 to 13.14 jovian radii from Jupiter. The data are given in a Jupiter-centred right-handed spherical coordinate system ( $r, \theta, \phi$ ) with  $r$  the radial distance,  $\theta$  the angle from the spin axis, and  $\phi$  the azimuthal angle. This is a variant of System III (1996)<sup>14</sup> with  $\phi$  increasing westward. The ten-hour periodicity arises from Jupiter's rotation. Closest approach to Ganymede was at 06:29:07 UT. All times are given as spacecraft event time, which is universal time at the spacecraft. The magnetic field vector is  $\mathbf{B} = (B_r, B_\theta, B_\phi)$ .

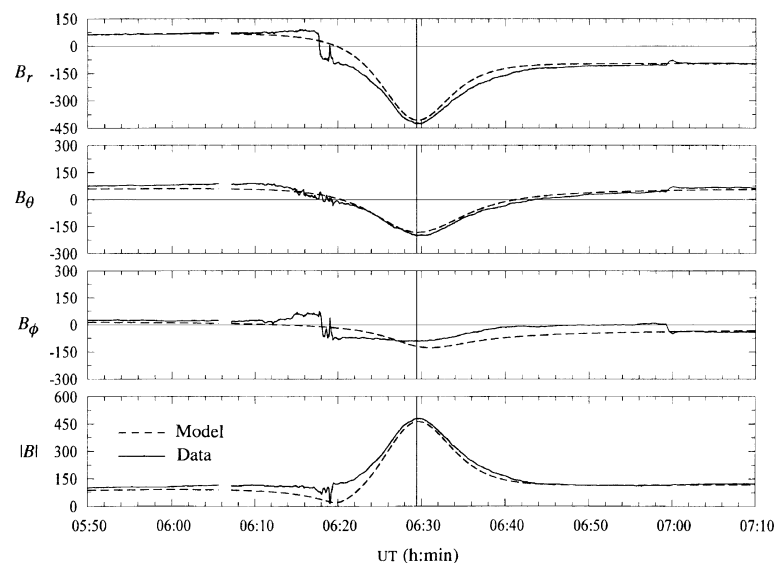


FIG. 2 Magnetic-field components and magnitude (solid lines) from 05:50 UT to 07:10 UT on 27 June 1996. The data are given in a Ganymede-centred coordinate system referenced to Ganymede's spin axis with  $r$  the radial distance,  $\theta$  the angle from an axis parallel to Jupiter's spin axis and through Ganymede's centre, and  $\phi$  the azimuthal angle, increasing eastward. Galileo's radial distance from the centre of Ganymede varied from  $6.85 R_G$  (radius of Ganymede, 2,634 km) at 05:50 UT to  $1.32 R_G$  at closest approach (marked by a vertical line) and out to  $5.47 R_G$  at 07:00 UT. Dashed lines show the superposition of a model of the jovian field<sup>3</sup> and the field of a Ganymede-centred magnetic moment described in the text. The data resolution is 0.333 s between 06:07 and 06:44 UT. Elsewhere the data resolution is 24 s.

north pole  $10^\circ$  radially outward). This model neglects minor components of both the external field and the dipole moment out of the  $y$ - $z$  plane (the coordinates are defined in Fig. 3 legend). A significant element of the schematic is the presence of field lines linked to Ganymede at both ends out to  $\sim 2R_G$  (where  $R_G$  is the radius of Ganymede), implying that Ganymede carves out its own magnetosphere within the jovian magnetosphere. The interpretations of plasma wave emissions by Gurnett<sup>7</sup> are consistent with this interpretation.

Figure 5 shows (heavy lines) the separatrix that encloses Ganymede's magnetosphere, identified as the region in which field lines link to Ganymede at least once. Galileo crossed into the Ganymede magnetosphere very near the boundary between field lines that intersect Ganymede's surface only once and field lines that intersect Ganymede's surface twice (see the trajectory in Fig. 5) and then passed through a region analogous to the cusp (or polar cusp) of a conventional magnetosphere<sup>8</sup>. The separatrix intersects the inbound trajectory at 06:20 UT, quite close to the time of the rather abrupt field rotation observed at  $\sim 06:17:45$  UT, and intersects the outbound trajectory at 07:00 UT just at the time a small rotation was observed. The boundary is analogous to the magnetopause of a conventional magnetosphere, and its signature is also clear in the plasma wave data<sup>7</sup>. The trajectory passed through the magnetic neutral line in the schematic simultaneous with crossing of the inbound separatrix. In the data, the field magnitude dropped to 12.85 nT consistent with a near-neutral line encounter at 06:19:06 UT, more than one minute after the field rotation.

We have analysed the field rotation for the inbound magnetopause crossing. The normal to the surface lies almost in the  $y$ - $z$  plane of Fig. 5a and is rotated radially outwards from the  $z$ -axis by  $33^\circ$ . This orientation suggests that in a more realistic model, the dipole centre might be shifted slightly towards positive  $z$ , the dimple in the separatrix would shift upward, and the trajectory would cross the separatrix just below the dimple. The small shift would produce a delay between the crossing of the separatrix and the encounter with the neutral line. It would account for the orientation of the magnetopause boundary during the inbound crossing, and it would hardly affect the outbound crossing. (Because the rotation at the outbound magnetopause is small, we are not able to evaluate the normal from the low-resolution data.)

It is not clear that we are justified in taking the details of a vacuum superposition model as far as has been done in the above analysis, but, because the ambient jovian electron density was probably  $\leq 1 \text{ cm}^{-3}$ , it is likely that neither the Alfvénic Mach number (flow speed/Alfvén speed) nor the plasma  $\beta$  (thermal pressure/magnetic pressure) was large enough for plasma effects to displace the boundary significantly. However, the Ganymede magnetosphere must divert the jovian plasma around the  $\sim 4R_G$  (diameter) magnetic obstacle. This region of diverted flow is analogous to a traditional magnetosheath, although the diverted flow is not bounded by a shock. Just before the magnetopause crossing, low-frequency fluctuations were observed as is common in a magnetosheath. Elsewhere fluctuations are very small, although the time resolution of the data was sufficient to detect fluctuations on the scale of seconds between 06:07 UT and 06:44 UT. The absence of fluctuations suggests low plasma pressure within the magnetosphere, although a peak density of  $>45 \text{ cm}^{-3}$  has been reported<sup>7</sup>.

The dipole moment of Ganymede ( $1.4 \times 10^{13} \text{ T m}^3$  or  $1.4 \times 10^{20} \text{ A m}^2$ ) is close to that inferred for Io<sup>1,9</sup>. Thus Ganymede, whose angular momentum is also close to that of Io, follows the trend of the relation between the magnetic moment and the angular momentum for magnetized planets suggested by Blackett<sup>10</sup>. However, the discovery of an internal field at Ganymede does not bear directly on the interpretation of the signature at Io as the properties of the two bodies differ greatly. In some ways, the conditions at Io seem more favourable for field generation than those at Ganymede. Density is higher, a large core is known to be

present<sup>11</sup>, rotation is faster, and there is a source of heat that could drive convection, even though the heat is not deposited directly in the core. However, as details of the heating and transport processes are likely to be very different at the two jovian satellites, the discovery of a Ganymede field does little to support the arguments<sup>1,9</sup> for an internal magnetic field of Io.

Given that the dipole moments are comparable, it may seem puzzling that the evidence for an internal field at Ganymede is unambiguous whereas the evidence for an internal field at Io, though compelling, is not unambiguous. The ambiguity arises both because the ratio of the magnitudes of the nominal surface equatorial magnetic field to the ambient jovian magnetic field is smaller by almost an order of magnitude at Io than at Ganymede and because the signature near Io is partially obscured by strong perturbations from ion pickup and charge exchange.

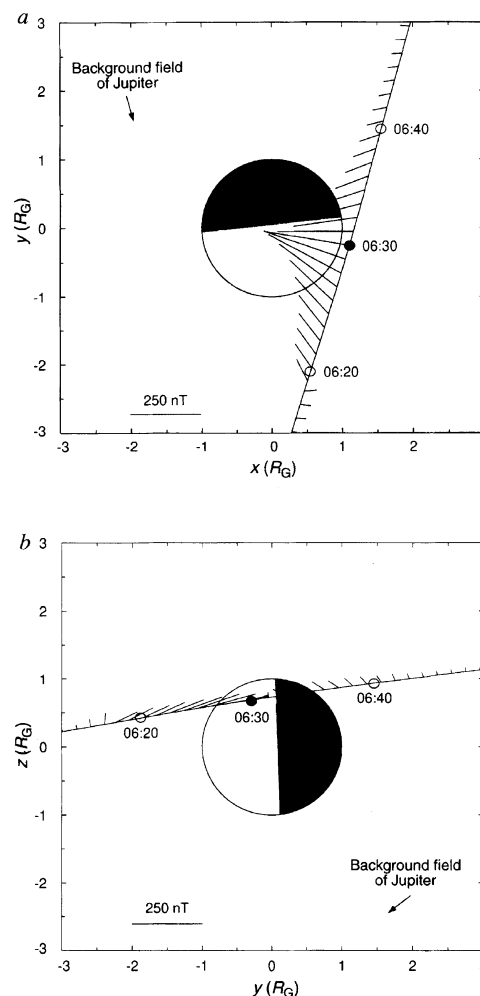
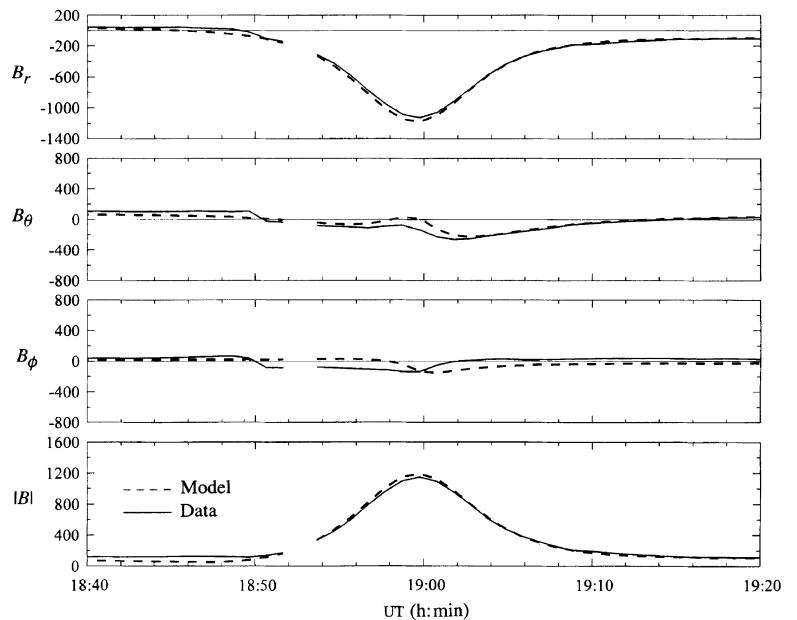


FIG. 3 Galileo's (27 June 1996) inbound towards Jupiter in the region near Ganymede (large circle, Ganymede; small circles, Galileo). The filled circle is near the closest approach to Ganymede. The plots use a coordinate system referenced to the direction of co-rotation (along  $\hat{x}$ ) and the spin axis of Jupiter, effectively the spin axis of Ganymede (along  $\hat{z}$ ). The unperturbed background field lies in the  $y$ - $z$  plane roughly  $50^\circ$  outward from  $-\hat{z}$ ;  $\hat{y}$  is positive inward towards Jupiter. a,  $x$ - $y$  projection, indicating the flow direction. The lines rooted along the trajectory are proportional to the projection of  $\mathbf{B} - \mathbf{B}_{\text{model}}$  of Fig. 2 and the scale for the field perturbations is indicated. Key times are given. The projection direction of the background field is also shown. The night side of Ganymede is shaded. The terminator was crossed close to the centre of the wake, with the sunlit side corresponding to negative values of  $y$ . b,  $y$ - $z$  projection of the trajectory and the perturbation field vectors. Note that the trajectory passes principally above Ganymede's equator.

FIG. 4 Magnetic field components and magnitude (solid lines) from 18:40 to 19:20 UT on 6 September 1996 during Galileo's second fly-by of Ganymede. The coordinate system is defined in Fig. 2 legend. A short gap in the data removes artefacts associated with a programmed gain change. (The gap is covered in the recorded data.) The coordinate system is the same as in Fig. 2. Galileo's radial distance from the centre of Ganymede varied from  $3.67 R_G$  at 18:40 UT to  $\sim 1.10 R_G$  at closest approach and out to  $3.74 R_G$  at 19:20 UT. Dashed lines show the superposition of the model fields discussed in the text. The data resolution is  $\sim 1$  minute.



The source of Ganymede's magnetic field could be dynamo action in a molten iron core (or a salty-water internal ocean) or remanent magnetization in its interior. Ganymede's internal structure and thermal state determine which of these possibilities is the most likely. Schubert *et al.*<sup>12</sup> have considered how the field might be generated by dynamo action in an iron core or a watery mantle. The magnitude of Ganymede's magnetic field, almost an order of magnitude larger at the satellite's pole than the ambient jovian magnetic field, is in accord with theoretical expectations for a dynamo-generated field as is the direction of the dipole axis approximately aligned with the rotation axis<sup>12</sup>. The dominantly

dipolar character of the field is consistent with generation deep within the body<sup>13</sup>. The large ratio between the polar field and the ambient field of the jovian magnetosphere at Ganymede cannot be explained by simple reactive processes such as paramagnetism or magneto-convection.

Remanent magnetization, though unlikely, cannot be ruled out completely. Whether in a core below the Curie temperature or in a magnetized shell in the interior of the moon, iron-rich material with a magnetic moment per unit volume  $\mu = 40\text{--}80 \text{ A m}^{-1}$  would produce the observed dipole moment. The external field required to account for such strong magnetization is in excess of the field

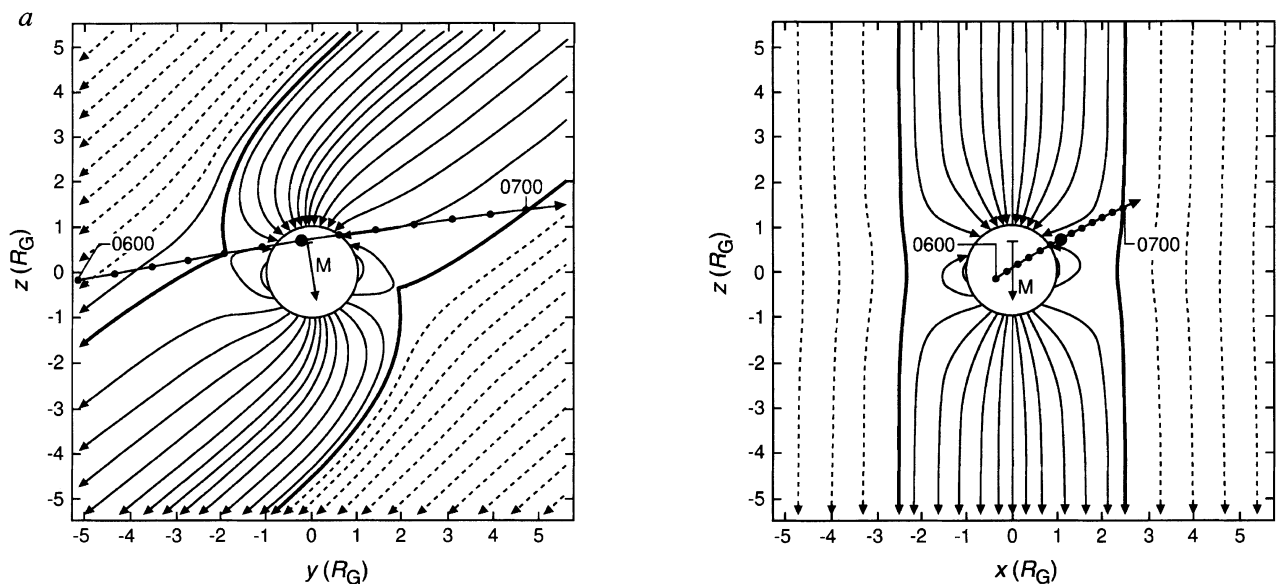


FIG. 5 Field lines in a vacuum superposition of a uniform external magnetic field of 120 nT lying in the  $y$ - $z$  plane and tilted by  $50^\circ$  outward from  $-z$  (a good approximation to the local value of the KK96 model field) and the field of a Ganymede-centred magnetic dipole with equatorial surface-field strength of 700 nT tilted  $10^\circ$  inward from  $-z$ . *a*, Field lines in the  $y$ - $z$  plane. *b*, Field lines in the  $x$ - $z$  plane. In both cases the projection of Galileo's trajectory is shown with dots every 5 minutes along the trajectory from 06:00 to 07:00 UT on 27 June 1996. Closest approach is marked with a

large dot. Note that the projection in *a* appears to place closest approach at high latitude, but the projection in *b* makes clear that the actual latitude is much lower. The separatrices between field lines linked to Ganymede and field lines that do not intersect the moon, effectively the magnetopause, are shown as heavy lines. Dashed lines are jovian field lines not linked to Ganymede. Solid lines are field lines with at least one end on Ganymede. An arrow marked *M* is aligned with Ganymede's magnetic moment.

near Ganymede in its present environment, but cannot be ruled out during its evolution. The inferred values cannot be rejected as impossibly large because the natural remanent magnetization of iron-rich meteorites can be this large in some cases.

We note that the presence of a strong internal field carries significant implications for the form of plasma flow near Ganymede. There should be no direct access of torus plasma to the surface other than in regions near the poles. Thus, deposits of sulphur-rich material from the torus should be localized near the poles. Sputtering of neutral atoms or molecules from Ganymede or its atmosphere would occur only in the polar regions, and this might inhibit significant neutral cloud formation and would certainly impose constraints on the cloud shape near the source. □

Received 30 September; accepted 5 November 1996.

1. Kivelson, M. G. *et al. Science* **273**, 337–340 (1996).
2. Kivelson, M. G., Khurana, K. K., Means, J. D., Russell, C. T. & Snare, R. C. *Space Sci. Rev.* **60**, 357–383 (1992).
3. Khurana, K. K. *J. Geophys. Res.* (submitted).
4. Connerney, J. E. P. in *Planetary Radio Emissions III* (eds Rucker, H. O., Bauer, S. J. & Kaiser, M. L.) 13–33 (Osterreichischen Akademie der Wissenschaften, Vienna, 1992).
5. Neubauer, F. M. *J. Geophys. Res.* **85**, 1171–1178 (1980).
6. Southwood, D. J., Kivelson, M. G., Walker, R. J. & Slavin, J. A. *J. Geophys. Res.* **85**, 5959–5968 (1980).
7. Gurnett, D. A., Kurth, W. S., Roux, A., Bolton, S. J. & Kennel, C. F. *Nature* **384**, 535–537 (1996).
8. Hughes, W. in *Introduction to Space Physics* (eds Kivelson, M. G. & Russell, C. T.) 227–287 (Cambridge Univ. Press, New York, 1995).
9. Kivelson, M. G., Khurana, K. K., Walker, R. J. & Warnecke, J. & Russell, C. T. *Science* **274**, 396–398 (1996).
10. Blackett, P. M. S. *Nature* **159**, 658 (1947).
11. Anderson, J. D., Shogren, W. L. & Schubert, G. *Science* **272**, 709–711 (1996).
12. Schubert, G., Zhang, K., Kivelson, M. G. & Anderson, J. D. *Nature* **384**, 544–545 (1996).
13. Elphic, R. C. & Russell, C. T. *Geophys. Res. Lett.* **5**, 211–214 (1978).
14. Dressler, A. J. in *Physics of the Jovian Magnetosphere* (ed. Dressler, A. J.) 498–504 (Cambridge Univ. Press, New York, 1983).

ACKNOWLEDGEMENTS. We thank S. Joy and A. Frederick for assistance in data preparation; R. L. Snare, J. Means, R. George, T. King and R. Silva for their varied contributions to the success of this effort; Y. Mei and D. Bindschadler for their support of magnetometer planning; V. Vasyliunas for discussions; and D. Stevenson for criticism. This work was supported by the Jet Propulsion Laboratory.

CORRESPONDENCE should be addressed to M.G.K. (e-mail: mkivelson@igpp.ucla.edu).

## Gravitational constraints on the internal structure of Ganymede

J. D. Anderson\*, E. L. Lau\*, W. L. Sjogren\*, G. Schubert† & W. B. Moore†

\* Jet Propulsion Laboratory, California Institute of Technology, Pasadena, California 91109-8099, USA

† Department of Earth and Space Sciences, Institute of Geophysics and Planetary Physics, University of California, Los Angeles, California 90095-1567, USA

**BEFORE the arrival of the Galileo spacecraft in the jovian system, there was little information on the interior structure of Jupiter's largest moon, Ganymede. Its mean density (1,940 kg m<sup>-3</sup>), determined by the Pioneer and Voyager spacecraft<sup>1–3</sup>, implies a composition that is roughly 60% rock and 40% ice, which could be uniformly mixed or differentiated into a rocky core and icy mantle<sup>4</sup>. Here we report measurements by the Galileo spacecraft of Ganymede's overall density and the spherical harmonics,  $J_2$  and  $C_{22}$ , of its gravitational field. These data show clearly that Ganymede has differentiated into a core and mantle. Combined with the recent discovery of an intrinsic magnetic field<sup>5,6</sup>, our gravity results suggest that Ganymede has a metallic core of radius 400–1,300 km surrounded by a silicate mantle, which is in turn enclosed by an ice shell ~800 km thick. Depending on whether the core is pure iron or an alloy of iron and iron sulphide, it could account for as little as 1.4% or as much as one-third of the**

**total mass. If the ice were stripped away, Ganymede could look much like Io<sup>7</sup> in terms of its size and internal mass distribution.**

The data were analysed by fitting a parametrized orbital model to the radio Doppler data by weighted nonlinear least squares<sup>8–10</sup>. The two encounters between Galileo and Ganymede (on 27 June and 6 September 1996) were analysed independently. Ganymede's external gravitational field was modelled by the standard spherical harmonic representation of the gravitational potential<sup>11</sup>. Because we assumed that the orientation of Ganymede's principal axes is known, only two non-zero coefficients ( $J_2$  and  $C_{22}$ ) were included in the model. All other harmonic coefficients were assumed to be exactly equal to zero. The two included coefficients measure the contributions to the gravitational potential of the spherical harmonics of degree  $l$  and order  $m$  for  $l = 2, m = 0$  and  $l = 2, m = 2$ , respectively. In terms of spherical coordinates fixed in the body of Ganymede (radius  $r$ , latitude  $\phi$ , and longitude  $\lambda$ ), where longitude is measured from the Ganymede–Jupiter line in an equatorial system defined by Ganymede's spin axis, and  $r$  is the radial distance from Ganymede's centre of mass, the gravitational potential is

$$V = \frac{GM}{r} \left[ 1 - \frac{1}{2} J_2 \left( \frac{R}{r} \right)^2 (3 \sin^2 \phi - 1) + 3 C_{22} \left( \frac{R}{r} \right)^2 \cos^2 \phi \cos 2\lambda \right] \quad (1)$$

where  $G$  is the gravitational constant, and  $M$  and  $R$  are the mass and radius of the satellite. The two encounters were intentionally targeted to optimize gravitational field measurements; the first was a near-equatorial pass at an altitude of 835 km, while the second was a near-polar pass at an altitude of 261 km. The closest-approach location for the first was at  $\phi = 30.394^\circ$  and  $\lambda = 112.129^\circ$  (west longitude), while the second was at  $\phi = 79.282^\circ$  and  $\lambda = 122.444^\circ$ . The first encounter was most sensitive to  $C_{22}$ , while the second was most sensitive to  $J_2$ . However, for both encounters the two gravity coefficients were highly correlated, so we imposed the *a priori* hydrostatic constraint that  $J_2$  is exactly 10/3 of  $C_{22}$ .

Gravity results for the two encounters are summarized in Table 1. Although the two gravity coefficients, because of the 10/3 constraint, were perfectly correlated *a priori*, the correlation after fitting the data is significantly less than unity for both encounters. This implies that there is considerable freedom for the two coefficients to differ from their hydrostatic values. To the contrary, it can be concluded from Table 1 that the non-hydrostatic perturbation to the second-degree field is only 0.2% with  $1\sigma$  uncertainty of 1.9%. It is highly unlikely that non-hydrostatic components contribute more than 6% to the Ganymede second-degree gravity field.

The value of  $GM$  is found to be  $9,886.6 \pm 0.5 \text{ km}^3 \text{ s}^{-2}$ . Masses derived from  $GM$  determinations depend on the gravitational constant  $G$ . The currently accepted value<sup>12</sup> is  $(6.672559 \pm 0.00085) \times 10^{-20} \text{ km}^3 \text{ s}^{-2} \text{ kg}^{-1}$ . This yields a mass of  $(1.48167 \pm 0.00020) \times 10^{23} \text{ kg}$  for Ganymede. Under the assumption that the volume of Ganymede is equal to that of an equivalent sphere of radius  $2,634 \pm 10 \text{ km}$  (ref. 13) its mean density is  $1,936 \pm 22 \text{ kg m}^{-3}$ , where the uncertainty is determined by the uncertainty in the radius.

Formal error estimates from the least-squares covariance matrix are based on an assumption of independent measurements drawn from a gaussian noise distribution. The reduced Galileo radio Doppler data are gaussian, but their power spectral density follows an  $f^{-2/3}$  law arising from propagation of the radio carrier wave through solar plasma<sup>14</sup>. Here  $f$  is the Fourier frequency, not the 2.3 GHz frequency of the radiowave. The variance of spectral estimates of a signal roughly follows the same power-law dependence as the noise spectrum, so the Galileo gravity signals are better determined at higher Fourier frequencies. Our data weighting, with an assumed variance approximately equal to the variance of the Doppler residuals ( $0.04 \text{ mm}^2 \text{ s}^{-2}$  at a sample interval of 60 s), is about right for the Ganymede gravity signals, where the peak